Development of a Substrate-Based Cyclic Phosphopeptide Inhibitor of Protein Phosphatase 2Cδ, Wip1[†]

Hiroshi Yamaguchi,[‡] Stewart R. Durell,[‡] Hanqiao Feng,[§] Yawen Bai,[§] Carl W. Anderson,[||] and Ettore Appella*[,‡]

Laboratory of Cell Biology and Laboratory of Biochemistry, National Cancer Institute, National Institutes of Health, Bethesda, Maryland 20892, and Biology Department, Brookhaven National Laboratory, Upton, New York 11973

Received July 5, 2006; Revised Manuscript Received August 22, 2006

ABSTRACT: The wild-type p53-induced phosphatase, Wip1 (PP2Cδ or PPM1D) is a member of the protein phosphatase 2C (PP2C) family and functions as a negative regulator of the p38 MAP kinase-p53 signaling pathway. *PPM1D* is amplified or Wip1 is overexpressed in several human cancers, and it acts as a weak oncogene. Although inhibition of Wip1 may have therapeutic value, no specific inhibitors are available. In this study, we designed phosphopeptide inhibitors for Wip1 on the basis of its optimal substrate sequence. We found that phosphoserine-containing diphosphorylated peptides with the sequence pS*X*pY inhibited Wip1 phosphatase activity, whereas phosphothreonine-containing peptides with the sequence pT*X*pY were physiological substrates. Moreover, the *X* residue in the pS*X*pY sequence modulated inhibitor activity, and β-branched amino acid-substituted (Ile or Val) phosphopeptides showed high inhibitory potencies. A thioether cyclic phosphopeptide c(MpSIpYVA) had a K_i <1.0 μM. Two serine/threonine phosphatases, PP2Cα and PP2A, were not significantly inhibited by the cyclic phosphopeptide with a nonhydrolyzable phosphoserine mimetic. A homology model of Wip1 bound to a cyclic phosphopeptide and site-directed mutagenesis helped to identify residues important for Wip1 inhibitor selectivity among the PP2C family. These results provide the first proof of concept of a specific inhibitor of the catalytic site of Wip1 and should be useful for developing potential anti-cancer drugs.

The wild-type p53-induced phosphatase Wip1[1] (PP2Cδ or PPM1D) is a member of the protein phosphatase 2C (PP2C) family, and its expression is induced by the p53 tumor suppressor after DNA damage, including that caused by ionizing radiation or UV light (*1*, *2*). The p38 mitogen-activated protein (MAP) kinase controls cellular pathways for proliferation, differentiation, development of the inflammatory response, and apoptosis (*3*). Like PP2Cα, another member of the PP2C family, Wip1 inactivates p38 MAP kinase through dephosphorylation of phosphothreonine in the pTGpY sequence of its regulatory site (*2*). Because phosphorylated p38 MAP kinase phosphorylates and activates p53 to cause cell cycle arrest or apoptosis in response to DNA damage (*4*−*6*), Wip1 controls a feedback loop in the p38 MAP kinase-p53 signaling pathway (*2*). Wip1 also interacts with a nuclear isoform of uracil DNA glycosylase (UNG2) and suppresses base excision repair through phosphothreonine dephosphorylation of its pTLpY sequence (*7*). It was recently reported that Wip1 dephosphorylates the phosphoserine of the pSQ sequence of p53 Ser15 and Chk1 Ser345 (*8*) and the phosphothreonine in the pTQ sequence of Chk2 Thr68 (*9*), suggesting that Wip1 may have an important role in controlling cell cycle checkpoints in response to DNA damage.

PPM1D, the gene that encodes Wip1, is amplified or overexpressed in several human cancers such as breast cancer, neuroblastomas, and ovarian clear cell adenocarcinoma (*10*−*13*), and *PPM1D* complements the oncogenes *Ras*, *Myc*, and *Neu* for the cellular transformation of primary mouse embryo fibroblasts (*11*). Disruption of *PPM1D* activates not only p53 but also the $p16^{INK4a}$-$p19^{ARF}$ pathways through p38 MAP kinase signaling (*14*). Although these studies suggest that inhibiting Wip1 activity or expression of the *PPM1D* gene may be an effective strategy for treating certain types of cancer, specific inhibitors of Wip1 or other members of the PP2C family have not been reported (*15*).

We recently demonstrated that Wip1 utilizes as a specific substrate the phosphorylated threonine in the pT*X*pY sequence of p38 MAP kinase and UNG2 (*16*). Wip1 prefers diphosphorylated peptides rather than monophosphorylated peptides, and an optimal substrate sequence is X_{-1}-pT-X_{+1}-pY-X_{+3}, where X_{-1}, X_{+1}, and X_{+3} denote any amino acid, any aliphatic amino acid, and any amino acid except proline,

[†] H.Y., S.R.D., H.F., Y.B., and E.A. were supported by the Intramural Research Program of the National Institutes of Health, National Cancer Institute. C.W.A. was supported in part by a Laboratory Directed Research and Development Award at the Brookhaven National Laboratory under contract with the U.S. Department of Energy.

* To whom correspondence should be addressed. Tel: 301-402-4177. Fax: 301-496-7220. E-mail: appellae@pop.nci.nih.gov.

[‡] Laboratory of Cell Biology, National Institutes of Health.

[§] Laboratory of Biochemistry, National Institutes of Health.

[||] Brookhaven National Laboratory.

[1] Abbreviations: Abu, 2-aminobutytic acid; CD, circular dichroism; Cha, cyclohexylalanine; F_2Pab, L-2-amino-4-phosphono-4,4-difluorobutanoic acid; Fmoc, 9-fluorenylmethoxycarbonyl; GST, glutathione *S*-transferase; HSQC, heteronuclear single quantum correlation; MAP, mitogen-activated protein; Nle, norleucine; NMR, nuclear magnetic resonance; NOE, nuclear Overhauser effect; Nva, norvaline; PP2C, protein phosphatase 2C; pX, phosphorylated amino acid; ROESY, rotational nuclear Overhauser effect spectroscopy; RP-HPLC, reversed-phase high-performance liquid chromatography; TOCSY, total correlation spectroscopy; UNG2, nuclear isoform of uracil DNA glycosylase; Wip1, wild-type p53-induced phosphatase.

10.1021/bi061356b CCC: $33.50
Published on Web 10/17/2006

respectively. The *X* residue in the pT*X*pY sequence affects the substrate's affinity for Wip1 (*16*). We found that the optimal substrate sequence of Wip1 differs from that of PP2Cα (*16*). It is expected that an inhibitor binding to the catalytic site of Wip1 would show high selectivity. In this study, we designed and synthesized a peptide inhibitor on the basis of Wip1 substrate specificity for the catalytic site. We report here that peptides with a pS*X*pY sequence inhibit Wip1 phosphatase activity, although peptides or proteins with a pT*X*pY sequence are substrates. Moreover, we found that thioether cyclic phosphopeptides with a pSIpY sequence show an even higher inhibitory activity (K_i of <1 μM), and we developed a nonhydrolyzable phosphoserine mimetic-substituted derivative that shows high selectivity toward Wip1.

EXPERIMENTAL PROCEDURES

Protein Expression and Purification. The *N*-terminal histidine-tagged, catalytic domain of human Wip1 (residues 1−420), rWip1, and the K238Q, K238D, and R110E mutants were expressed in *Escherichia coli* BL21(DE3) and purified as previously reported (*16*). The PP2A catalytic subunit, PP2Cα and the full-length p38α(180pT 182pY) phosphoprotein were purchased from Promega (Madison, WI) or Calbiochem (La Jolla, CA), respectively. The *N*-terminal GST-tagged, full-length p38α and MKK6 were purchased from Upstate Biotechnology (Charlottesville, VA).

Peptide Synthesis and Purification. Peptides were synthesized by the solid-phase method with 9-fluorenylmethoxycarbonyl (Fmoc) chemistry. Phosphoamino acids were coupled as Fmoc-Thr[PO(OBzl)OH]-OH, Fmoc-Ser[PO(OBzl)OH]-OH, and Fmoc-Tyr(PO_3H_2)-OH (Novabiochem, San Diego, CA). L-2-Amino-4-phosphono-4,4-difluorobutanoic acid (F_2Pab) was coupled as Fmoc-F_2Pab-OH (AnaSpec Inc., San Jose, CA). Acetylation of the *N*-terminus was achieved with acetic anhydride in the presence of 4-methylmorpholine. The thioether cyclic peptides were synthesized as described previously (*17*). The peptides were cleaved with 95% trifluoroacetic acid, 2.5% triisopropylsilane, and 2.5% water and then purified by reversed-phase high-performance liquid chromatography (RP-HPLC) on a C-4 or C-18 column with 0.05% trifluoroacetic acid/water/acetonitrile. The purity of the peptides was determined to be >95% by analytical RP-HPLC. The masses of peptides were confirmed by matrix-assisted laser desorption ionization time-of-flight mass spectrometry (Micromass, Beverly, MA).

Phosphatase Assay. Phosphatase activity was measured by a malachite green/molybdate-based assay (*16*, *18*, *19*). A screening assay was carried out in buffer A (50 mM Tris-HCl at pH 7.5, 0.1 mM EGTA, 0.02% 2-mercaptoethanol, 40 mM NaCl, and 30 mM $MgCl_2$). rWip1 (18 nM) was incubated with 50 μM TDDEMpTGpYVAT substrate peptide (residues 175−185 in human p38α MAP kinase) and 100 μM phosphopeptide inhibitor for 20 min at 30 °C.

The IC_{50} values for inhibition of phosphatase activity by the phosphopeptide inhibitors were measured using 50 μM TDDEMpTGpYVAT substrate peptide in buffer A for 7 min at 30 °C. The phosphatase and phosphopeptide inhibitors were pre-equilibrated at 30 °C for 6 min. The inhibition percentages were estimated by eq 1.

$$\text{Inhibition (\%)} = 100[1 - (A - A_0)/(A_{100} - A_0)] \quad (1)$$

where A and A_{100} are absorbance intensities at 650 nm with or without the peptide inhibitor, respectively. A_0 is the absorbance of the sample without phosphatase. The IC_{50} values were estimated by a sigmoidal dose−response equation. The apparent inhibitory constant K_i values were estimated using eq 2 (*20*).

$$K_i = IC_{50}/(1 + [S]/K_m) \quad (2)$$

where [S] is the concentration of the substrate peptide, and K_m is the Michaelis constant.

Steady-State Kinetics Assay. Kinetics assays were carried out in the manner described above. The amount of phosphate released was calculated using a phosphate standard curve. To determine the kinetic parameters K_m and k_{cat}, the initial velocities (v) were measured at various concentrations of substrate peptide ([S]), and data were fitted to the Michaelis−Menten equation (eq 3).

$$v = k_{cat}[S]/(K_m + [S]) \quad (3)$$

For inhibitor experiments, the initial velocities were measured at various concentrations of the substrate peptide with a constant concentration of the inhibitor ([I]). Lineweaver−Burke plots were used to assess the type of inhibition. The K_{is} value was obtained by fitting the data to the competitive inhibition equation (eq 4).

$$v = k_{cat}[S]/(K_m(1 + [I]/K_{is}) + [S]) \quad (4)$$

Inhibition of Wip1-Catalyzed p38α Phosphoprotein Dephosphorylation by the Thioether Cyclic Phosphopeptide. The phosphorylated, full-length p38α(180pT 182pY) protein (150 nM) and rWip1 (150 nM) were combined with or without the cyclic phosphopeptide inhibitor. Reactions were carried out in 50 mM Tris-HCl at pH 7.5, 0.1 mM EGTA, 0.02% 2-mercaptoethanol, and 30 mM $MgCl_2$ at 30 °C for 30 min. The cyclic phosphopeptide and the rWip1 inhibitor were pre-equilibrated at 30 °C for 5 min. The reactions were terminated by adding 2× SDS−PAGE sample buffer. The samples were resolved by SDS−PAGE and transferred onto polyvinylidene difluoride membranes. After blocking with 4% BSA, membranes were probed with a polyclonal phospho-p38 antibody (Thr180/Tyr182; Cell Signaling Technology, Beverly, MA) followed by a peroxidase-conjugated secondary antibody (Amersham Bioscience, Piscataway, NJ) and chemiluminescent detection (Amersham Bioscience). The p38α protein level in each reaction was determined by Coomassie staining.

Kinase Assay. GST-p38α protein (150 nM) and MKK6 (30 nM) were combined with or without cyclic phosphopeptide inhibitors (100 μM). Reactions were carried out in buffer A with 100 μM ATP at 30 °C for 30 min. The reactions were terminated by adding 2× SDS−PAGE sample buffer. Samples were subjected to immunoblotting analysis using an anti-phospho-p38 antibody or a monoclonal GST antibody (26H1; Cell Signaling Technology) as described above.

Circular Dichroism (CD) Measurements. Far-UV CD spectra were measured on a JASCO J-715 spectropolarimeter (Easton, MD) using a quartz cuvette with a path length of 1

mm at 25 °C. Peptides were dissolved in buffer A at a concentration of 50 μM. Eight scans were averaged for each sample. The averaged blank spectrum (buffer A) was subtracted.

NMR Spectroscopy and Determination of Peptide Structure. NMR samples were prepared by dissolving the cyclic phosphopeptide inhibitor powder in 50 mM sodium acetate buffer (pH 5.0). NMR spectra were collected on a Bruker Avance-500 MHz spectrometer at 280 K. Homonuclear, 2D total correlation spectroscopy (2D TOCSY) (*21*), and 2D ^{13}C heteronuclear single quantum correlation (HSQC) (*22*) were used for the assignments of the peptide. The nuclear Overhauser effect (NOE)-derived distance restraints were determined from homonuclear 2D rotational nuclear Overhauser effect spectroscopy (ROESY) (*23*). The processing and analysis of the collected data were carried out with NMRPipe (*24*) and NMRView (Merck Research Laboratories) software packages.

The structures were calculated on the NIH Biowulf cluster with the program XPLOR-NIH version 2.13 (*25*). The upper distance bounds were set to different categories of <2.5, 2.5−3.5, 3.5−4.5, and 4.5−6.0 Å on the basis of the intensities of the NOEs. Calculations were performed using a standard simulated annealing protocol starting from random coordinates. Fifty conformers were calculated on the basis of 123 NOE-derived distance restraints. The 10 lowest-energy structures with no distance violations greater than 0.3 Å and no angle violations greater than 5° were accepted into the final ensemble.

Molecular Modeling and Computational Analysis. The 3D molecular models of the Wip1 protein and the linear and cyclic phosphopeptide inhibitors were developed as previously described (*16*). As before, the homology model of Wip1 did not include residues 239−263 of the protein sequence, which likely form a loop on the protein surface near the periphery of the catalytic site. That is, the average distance of the loop's *N*- and *C*-terminal anchors from the two metal atoms is approximately 16 Å. Unfortunately, this segment cannot be modeled with much confidence because it is unique among the sequence alignment of the PP2C family members (not shown) and, thus, lacks a conformational template from the PP2Cα crystal structure (*26*). Secondary structure prediction of this segment alone using a variety of methods suggests that it forms a β-hairpin loop (results not shown). However, what the protein-bound structure would be or how it would orient on the surface of Wip1 cannot be correctly predicted. Likewise, the observed waters in the catalytic site of the PP2Cα crystal structure (*26*) and possible repositioning of the His107 residue (His62 in PP2Cα) (*27*) were not carried-over to the Wip1 homology model because of structural uncertainty.

Docking simulations were performed and analyzed with the integrated AutoDock3 (*28*) and AutoDockTools (*29*) software packages. The simulations were setup using a variety of sampling grid sizes with the shortest side ranging from 27 to 38 Å. These distances were sufficient to permit the tested peptides to fully rotate during the docking conformational searches. The point spacing of each grid was kept at the default 0.375 Å, but a few different positions were used in centering over the catalytic site of Wip1 to reduce finite-grid artifacts. Minimums of 200 independent simulations were run for each peptide, with both random starting positions and a series of arbitrarily selected fixed positions over the catalytic site. Simulations of the cyclic peptides allowed for rotation of all of the single bonds of the side chains while keeping the circularized backbone in the minimized average conformation obtained by NMR. In contrast, simulations of the linear peptides allowed for free rotation around all non-amide backbone dihedrals in addition to the side chain single bonds. In all cases, the sampling was carried out with the Lamarckian genetic algorithm, with population sizes ranging from 50 to 150 individuals and the number of generations ranging from 1500 to 20 000. The default values were used for all other algorithmic parameters.

RESULTS

Inhibition of Phosphatase Activity of the Human Wip1 Catalytic Domain (rWip1) by Phosphopeptides. Both Wip1 and PP2Cα dephosphorylate the phosphothreonine residue of the pTGpY sequence from the p38 MAP kinase protein or its peptide *in vivo* and *in vitro* (*2*, *16*, *30*). However, a kinetics study using phosphopeptides showed that diphosphorylated peptides with a pT*X*pY sequence (*X* = glycine, alanine, or leucine) are better substrates for Wip1 than monophosphorylated peptides, whereas PP2Cα prefers monophosphorylated peptides with pT*X*Y or R*X*pT sequences (*16*). These results indicate that the optimal substrate sequence of Wip1 differs from that of PP2Cα. A homology model of Wip1 that was developed from the crystal structure of PP2Cα (*26*) showed that all of the metal-binding and directly adjacent residues in the catalytic sites of both Wip1 and PP2Cα are identical, whereas the residues surrounding the catalytic sites differ (*16*). Lysine 238 (K238) in human Wip1, located near the catalytic site, is unique among residues of the PP2C family. A docking model of Wip1 with the p38 substrate peptide (DEMpTGpYVA) and a point mutation study revealed that K238 interacts with the phosphotyrosine residue in the p38 peptide and plays an important role in substrate discrimination (i.e., preference for diphosphorylated substrates) (*16*). Therefore, we considered the possibility that a phosphotyrosine peptide might bind to the catalytic site of Wip1 and inhibit its phosphatase activity with high selectivity.

To confirm this possibility, we first tested the inhibition of the Wip1-catalyzed substrate peptide, TDDEM**pT**G**pY**-VAT, corresponding to p38α MAP kinase sequence residues 175−185 (human), by the phosphotyrosine peptide TDDEMTG**pY**VAT. In this experiment, we used the catalytic domain of human Wip1 (rWip1), which has phosphatase properties comparable to those of full-length Wip1 (*16*). As shown in Table 1, the phosphotyrosine peptide (row 2) slightly inhibited the activity of rWip1 relative to the nonphosphopeptide (row 1). Because rWip1 prefers diphosphorylated peptides, we also tested the inhibitory activity of a phosphoserine peptide with a pSGpY sequence that is not a substrate for rWip1 (Table 1 and ref *16*). Interestingly, the diphosphorylated peptide (row 3) showed higher inhibitory activity than that of the phosphotyrosine peptide (row 2) or the monophosphorylated phosphoserine peptide (row 4). These results indicate that phosphotyrosine peptides can inhibit the Wip1 phosphatase activity and that the diphosphorylated peptide with a pSGpY sequence had higher inhibition potency.

Table 1: Kinetics Parameters and Inhibitory Activities of Phosphopeptides

	phosphopeptide[a]	K_m (μM)	k_{cat} (s^{-1})	inhibition (%)[b]
1	TDDEMT-G-YVAT	ND[c]	ND[c]	0
2	TDDEMT-G-**pY**VAT	ND[c]	ND[c]	7 ± 2
3	TDDEM**pS**-G-**pY**VAT	ND[d]	ND[d]	15 ± 2
4	TDDEM**pS**-G−YVAT	ND[d]	ND[d]	7 ± 5
5	TDDEMpS-**A**-pYVAT	60 ± 11	1.8 ± 0.2	ND[c]
6	TDDEMpS-**V**-pYVAT	ND[d]	ND[d]	51 ± 0.4
7	TDDEMpS-**I**-pYVAT	ND[d]	ND[d]	54 ± 0.1
8	TDDEMpS-**L**-pYVAT	41 ± 14	0.8 ± 0.1	ND[c]
9	TDDEMpS-**D**-pYVAT	ND[d]	ND[d]	32 ± 1
10	TDDEMpS-**F**-pYVAT	ND[d]	ND[d]	0 ± 5
11	TDDEMpS-**K**-pYVAT	ND[d]	ND[d]	8 ± 2
12	TDDEMpS-**P**-pYVAT	ND[d]	ND[d]	26 ± 5
13	TDDEMpS-**Q**-pYVAT	10 ± 1	1.6 ± 0.03	ND[c]
14	TDDEMpS-**S**-pYVAT	86 ± 16	1.8 ± 0.2	ND[c]
15	TDDEMpS-**Abu**-pYVAT	38 ± 9	1.2 ± 0.1	ND[c]
16	TDDEMpS-**Nva**-pYVAT	17 ± 2	1.1 ± 0.03	ND[c]
17	TDDEMpS-**Nle**-pYVAT	13 ± 1	0.9 ± 0.02	ND[c]
18	TDDEMpS-**Cha**-pYVAT	ND[d]	ND[d]	40 ± 2

[a] The regions containing phosphorylated residues in the peptides are highlighted in gray, and substitutions are indicated by bold type. Abu, 2-aminobutytic acid; Nva, norvaline; Nle, norleucine; and Cha, cyclohexylalanine. [b] The results are presented as inhibitory activity relative to that in control incubations where the inhibitor was omitted. Concentrations of rWip1, phosphopeptide inhibitor, and the TDDEMpTGpYVAT substrate peptide were 18 nM, 100 μM, and 50 μM, respectively. The results show the means ± standard error of at least triplicate experiments. [c] Not determined. [d] The K_m and k_{cat} values could not be determined because of the high K_m. All assays were performed at 30 °C and pH 7.5.

Phosphopeptides that have a hydrophobic amino acid (alanine, leucine, or valine) at the *X* residue in the pT*X*pY sequence showed high affinity for rWip1 compared with those having pTGpY, pTEpY, or pTPpY sequences (*16*). Therefore, the *X* residue in the TDDEMpS*X*pYVAT diphosphorylated peptide was changed to several amino acids (rows 5−18 in Table 1). Because some of phosphopeptides could be potential substrates for rWip1, we first measured kinetic parameters for those phosphopeptides (Table 1). The hydrophobic amino acids (alanine, leucine, and 2-aminobutylic acid) or serine-substituted peptides were poor substrates compared to the TDDEMpTGpYVAT substrate peptide (K_m = 17 μM, k_{cat} = 0.8 s^{-1}). A glutamine-substituted peptide was a good substrate for rWip1 (row 13). The k_{cat}/K_m value for this peptide was increased by 3.4-fold compared to the TDDEMpTGpYVAT substrate peptide and is consistent with the recent finding that phosphoserine in the pSQ sequences of p53 and Chk1 are dephosphorylated by Wip1 (*8*). Norvaline- and norleucine-substituted peptides showed similar kinetic parameters to the TDDEMpTGpYVAT substrate peptide (rows 16 and 17). Other substituted peptides in Table 1 were not dephosphorylated by rWip1.

The inhibitory activities of phosphopeptides, except for the substrate peptides as described above, were next analyzed (Table 1). The β-branched amino acid (valine or isoleucine)-substituted peptides showed 3.5-fold higher inhibitory activity (rows 6 and 7) than that of the glycine-substituted peptide (row 3) while aspartic acid-, phenylalanine-, lysine-, or proline-substituted peptides showed lower inhibitory activity against rWip1 (rows 9−12). The activity of a more bulky amino acid (such as cyclohexylalanine-substituted peptide (row 18)) also was lower than that of valine- or isoleucine-substituted peptides. These results indicated that the *X* residue in the pS*X*pY sequence is important for modulating the inhibitory activity and also the substrate interaction with the enzyme. From these substituted peptides, TDDEMpSIpYVAT was used as a template for the subsequent development of inhibitors.

Inhibition by Thioether Cyclic Phosphopeptides with a pSIpY Sequence. To develop more potent and smaller sized inhibitors, one of the modifications frequently undertaken is to cyclize the peptide in order to decrease conformational flexibility (*17*). Therefore, the template phosphopeptide TDDEMpSIpYVAT was cyclized. Furthermore, to attain a small inhibitor, we synthesize truncated cyclic phosphopeptides by deleting residues from the *N*-terminus. For cyclization, a thioether linkage between the *N*-terminal acetyl residue and the side chain of the *C*-terminal cysteine was introduced (Figure 1A) because this is a simple reaction, and it is useful for further modifications at the *C*-terminus of the peptide.

Thioether cyclic phosphopeptides were compared with linear phosphopeptides that were blocked by acetylation at the *N*-terminus and by amidation at the *C*-terminus, respectively (Figure 1A). The modifications of linear peptides at both termini did not significantly affect their inhibitory activities in comparison with nonmodified peptides. For example, the activities of Ac-TDDEMpSIpYVAT-NH_2 and TDDEMpSIpYVAT were 58 and 54%, respectively, under the same conditions as those in Table 1. As shown in Figure 1B, the inhibitory activities of linear peptides (open bars) were slightly reduced by decreasing the chain-length. In contrast, the cyclization of peptides (closed bars), except for the cyclic pSIpYVAT peptide denoted as c(pSIpYVAT), enhanced the inhibitory activities compared to that of each linear peptide. The c(EMpSIpYVAT) and c(MpSIpYVAT) peptides exhibited especially significant enhancements of inhibitory activities. To compare the conformation of cyclic and linear peptides, CD spectra of c(MpSIpYVAT) and Ac-MpSIpYVAT-NH_2 were measured (Figure 1C). The linear peptide showed a negative band around 200 nm, which implies a nonordered structure. However, c(MpSIpYVAT) showed negative bands around 204 and 218 nm, characteristic of a β-turn (*31*), suggesting that the cyclization of peptides decreased their conformational flexibility, as expected.

To find a more potent and possibly smaller inhibitor, we next tested truncated peptides of c(MpSIpYVAT) by deleting residues from the *C*-terminus (Figure 2A). Peptides with one or two amino acids deleted from the *C*-terminus gave complete inhibitory activity against rWip1 under our assay conditions. Further deletion, as in c(MpSIpY), did not show an improvement of inhibitory activity. The IC_{50} values for the inhibition of rWip1 by the cyclic phosphopeptides were measured at a constant concentration of the TDDEMpTGpYVAT substrate peptide. As shown in Figure 2B and Table 2, the cyclic phosphopeptides inhibited rWip1 phosphatase activity in a dose-dependent manner, and we found a six-residue cyclic phosphopeptide c(MpSIpYVA) to be the most potent and smallest inhibitor of rWip1. The IC_{50} value of 3.7 μM was 37-fold better than that of an 11-residue cyclic phosphopeptide, c(TDDEMpSIpYVAT). These results indicate that cyclization of the phosphopeptide is effective not only in increasing the inhibitory activity but also in reducing the molecular size.

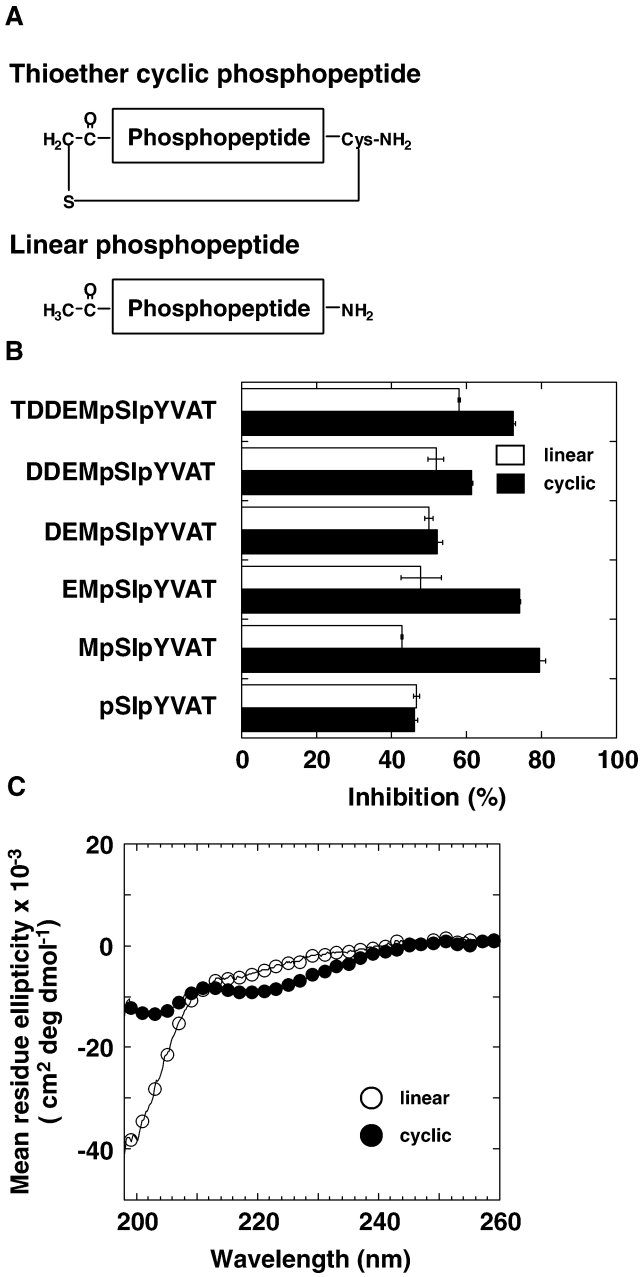

FIGURE 1: Inhibition of rWip1 by thioether cyclic and linear phosphopeptides. (A) Schematic representation of thioether cyclic and linear phosphopeptides. The thioether linkage was formed between the *N*-terminal acetyl residue and the side chain of a *C*-terminal cysteine amide. The *N*- and *C*-terminus of linear phosphopeptides were blocked by acetylation and amidation, respectively. (B) Comparison of the inhibition of rWip1 by thioether cyclic (closed bars) and linear (open bars) phosphopeptides with different chain-lengths using the substrate peptide, TDDEMpTGpYVAT. Concentrations of the inhibitors and substrate were 100 μM and 50 μM, respectively. The graph shows the average of at least duplicate experiments. All assays were performed at 30 °C and pH 7.5. (C) CD spectra of c(MpSIpYVAT) (●) and Ac-MpSIpYVAT-NH_2 (○) phosphopeptides in buffer (pH 7.5) at 25 °C. Peptide concentrations were 50 μM.

Characterization of a Thioether Cyclic Phosphopeptide c(MpSIpYVA). The phosphopeptide inhibitors in this study were designed as inhibitors of the catalytic site of Wip1. To confirm that c(MpSIpYVA) actually interacted with the catalytic site of rWip1, the inhibitory mechanism of c(MpSIpYVA) was studied. As expected, Lineweaver−Burke plots, using the TDDEMpTGpYVAT substrate peptide,

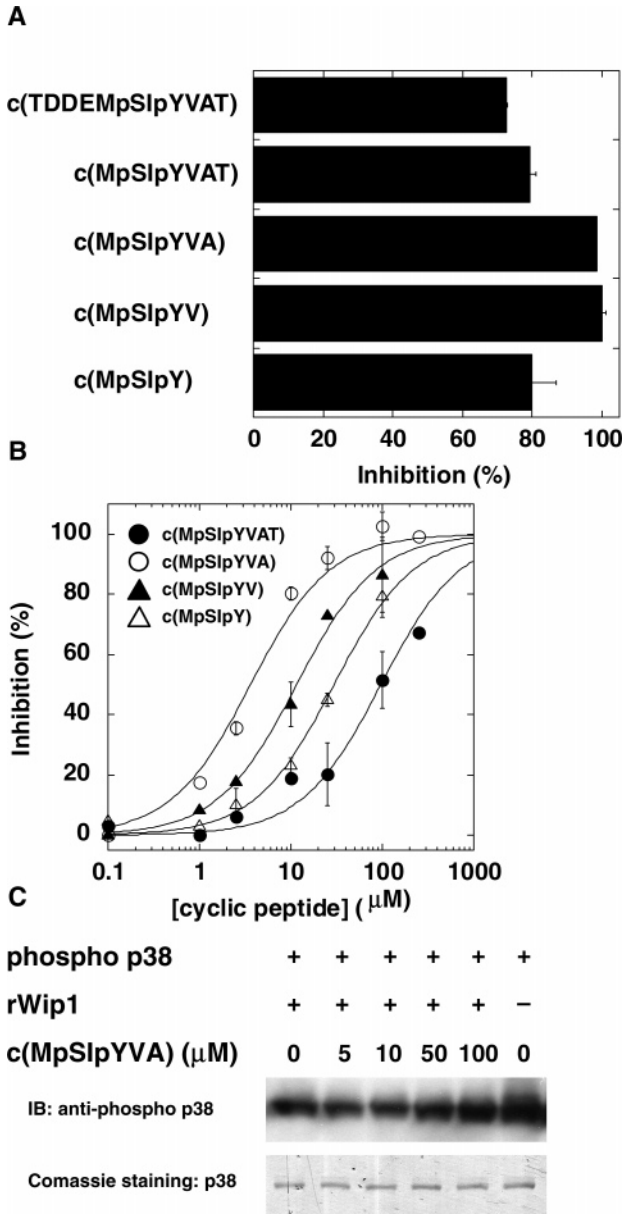

FIGURE 2: Inhibition of rWip1 phosphatase activity by the thioether cyclic phosphopeptides. (A) Inhibition by different chain-length thioether cyclic phosphopeptides (thioether cyclic peptides are denoted by c(peptide sequence)). Experimental conditions were the same as those in Figure 1B. (B) Concentration dependence of inhibition by thioether cyclic phosphopeptides: c(MpSIpYVAT) (●), c(MpSIpYVA) (○), c(MpSIpYV) (▲), and c(MpSIpY) (△). Concentration of the TDDEMpTGpYVAT substrate peptide was 50 μM. The data were fitted to the sigmoidal dose−response equation as described in Experimental Procedures. The graph shows the average of at least duplicate experiments. All assays were performed at 30 °C and pH 7.5. (C) Inhibition of the rWip1-catalyzed, full-length p38α(180pT 182pY) dephosphorylation by c(MpSIpYVA). The reaction mixture of rWip1 (150 nM) and p38α phosphoprotein (150 nM) was incubated with c(MpSIpYVA) (0, 5, 10, 50, and 100 μM) at 30 °C and pH 7.5 for 30 min. Dephosphorylation of the p38α phosphoprotein was determined by immunoblotting analysis using an anti-phospho-p38 antibody (top panel) that did not recognize the non-phosphorylated p38α protein (data not shown). The p38α protein level in each reaction was confirmed with Coomassie staining (bottom panel).

indicated that c(MpSIpYVA) is a competitive inhibitor (plots not shown) with a K_{is} of 0.7 μM. This value is consistent with the apparent K_i value (0.9 μM) from the IC_{50} value shown in Table 2, suggesting that c(MpSIpYVA) acts as a

Table 2: Inhibition of rWip1 Phosphatase Activity by Thioether Cyclic Phosphopeptides at 30 °C and pH 7.5[a]

cyclic phosphopeptide	IC_{50} (μM)	K_i (μM)
c(TDDEMpSIpYVAT)	138.4 ± 35.6	35.0
c(MpSIpYVAT)	99.9 ± 11.5	25.2
c(MpSIpYVA)	3.7 ± 0.2	0.9
c(MpSIpYV)	11.6 ± 1.0	2.9
c(MpSIpY)	29.4 ± 2.3	7.4

[a] The IC_{50} values for inhibition of rWip1 activity by the different cyclic peptides were estimated from dose−response phosphatase assays, and the apparent K_i values were estimated by eq 2 as described in Experimental Procedures. Thioether cyclic peptides are denoted by c(peptide sequence). The results show the average of at least duplicate experiments.

highly active inhibitor at the catalytic site. We next tested whether c(MpSIpYVA) could inhibit the rWip1-catalyzed, full-length p38α(180pT 182pY) dephosphorylation. Immunoblot analysis with an antibody that specifically recognizes the diphosphorylated form of the p38α protein indicated that c(MpSIpYVA) also inhibited rWip1 phosphatase activity toward the p38α protein in a dose-dependent manner (Figure 2C).

The conformation of c(MpSIpYVA) was investigated by CD and NMR spectroscopy. As shown in Figure 3A, the CD spectrum of c(MpSIpYVA) exhibited a negative band and a shoulder around 203 and 214 nm, which is indicative of a β-turn structure (*31*), and a positive band around 230 nm. This spectrum is different from that of c(MpSIpYVAT) (Figure 1C), which had weak inhibitor activity, or c(pSIpYVAT), which also had weak activity (Figure 1B) and the same number of amino acids as those of c(MpSIpYVA) (Figure 3A). The 3D structure of c(MpSIpYVA) obtained by NMR measurements is shown in Figure 3B. Specifically, nine independent models resulting from the structure determination process are superimposed to judge the flexibility of the molecule. All of the side chains project away from the backbone core. As can be seen, the conformation of the backbone (green) is highly constrained for this cyclic peptide. The largest motion occurs at the thioether sulfur atom (yellow) that links the ends of the peptide, and the backbone is bent at the thioether bond. The IpYVA four residues are involved in the β-turn structure, and this is consistent with the CD spectrum. The pSIpY three-residue stretch also assumes an approximate 3_{10}-helical conformation. Thus, these results indicate that forming a rigid backbone through appropriate length reduction and cyclization contributes to enhanced inhibitory activity.

Thioether Cyclic Phosphopeptide Inhibitor with a Phosphoserine Mimetic Shows Selectivity toward rWip1. To determine whether the activity of c(MpSIpYVA) is specific to rWip1, its inhibitory activity toward two other serine/threonine protein phosphatases, PP2Cα and PP2A, was evaluated. PP2A, which is in a different gene family (*32*), was not significantly inhibited by c(MpSIpYVA) (Table 3). However, PP2Cα, in the same family as that of Wip1, dephosphorylated the phosphoserine in c(MpSIpYVA). The estimated K_m and k_{cat} values were 11 μM and 2.0 s^{-1}, respectively, and the k_{cat}/K_m value was 8.3-fold higher than that of the TDDEMpTGpYVAT substrate peptide (K_m = 90 μM and k_{cat} = 2.0 s^{-1}), indicating that c(MpSIpYVA) was a better substrate of PP2Cα than TDDEMpTGpYVAT. To circumvent dephosphorylation by PP2Cα, we next synthesized c(MpSIpYVA) derivatives with a nonhydrolyzable phosphoserine mimetic. L-2-Amino-4-phosphono-4,4-difluorobutanoic acid (F_2Pab), which has a chemical structure similar to that of serine phosphate (Figure 4A), was introduced as a mimetic. F_2Pab-derived peptides are resistant to hydrolysis by cellular phosphatases, and, in contrast to methylene derivatives, the second ionization constant of the phosphonate (pKa2) is closed to that of the phosphate (*33*).

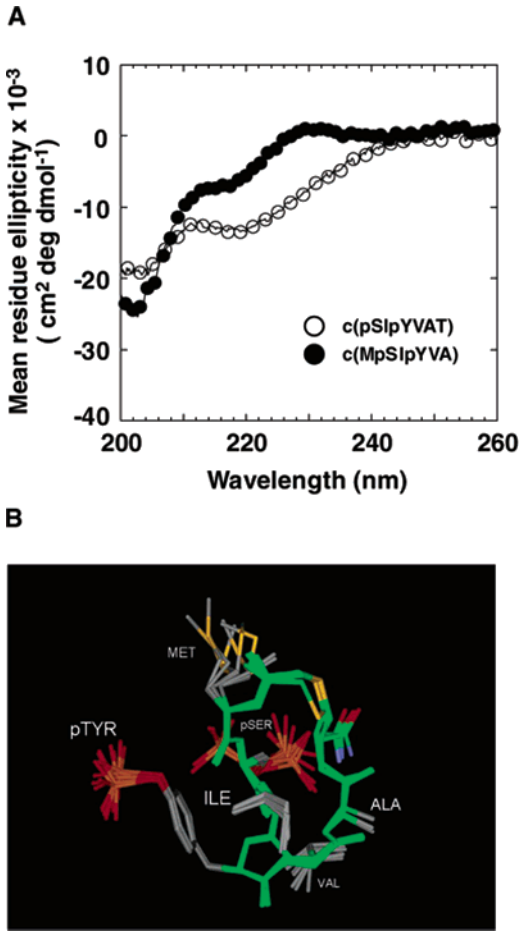

FIGURE 3: Solution structure of c(MpSIpYVA). (A) CD spectra of c(MpSIpYVA) (●) and c(pSIpYVAT) (○) phosphopeptides in buffer (pH 7.5) at 25 °C. Peptide concentration was 50 μM. (B) Superposition of nine independent models of c(MpSIpYVA) developed from NMR measurements as described in Experimental Procedures. The amino acid backbone atoms are colored green, and yellow is used to highlight the thioether sulfur. Of the side chains, carbon is gray, oxygen is red, phosphorus is orange, and sulfur is yellow. Additionally, red and blue denote the oxygen and nitrogen, respectively, of the *C*-terminal amine.

Table 3: Selectivity of Thioether Cyclic Phosphopeptides Toward Other Serine/Threonine Phosphatases

	IC_{50} (μM)[b]		
cyclic phosphopeptide[a]	rWip1	PP2Cα	PP2A
c(M**pS**IpYVA)	3.7 ± 0.2	[c]	>200
c(M**F_2Pab**IpYVA)	16.5 ± 4.5	>200	>200
c(M**E**IpYVA)	>200	>200	>200
c(M**D**IpYVA)	>200	>200	>200

[a] Phosphoserine and phosphoserine mimetic residues are indicated in bold. [b] The concentrations of the rWip1, PP2Cα, and PP2A catalytic domains were 18 nM, 17 nM, and 2.1 U/mL, respectively. Other conditions were the same as those in Figure 2B. The results show the average of at least duplicate experiments. [c] Substrate: K_m = 11 μM; k_{cat} = 2.0 s^{-1}.

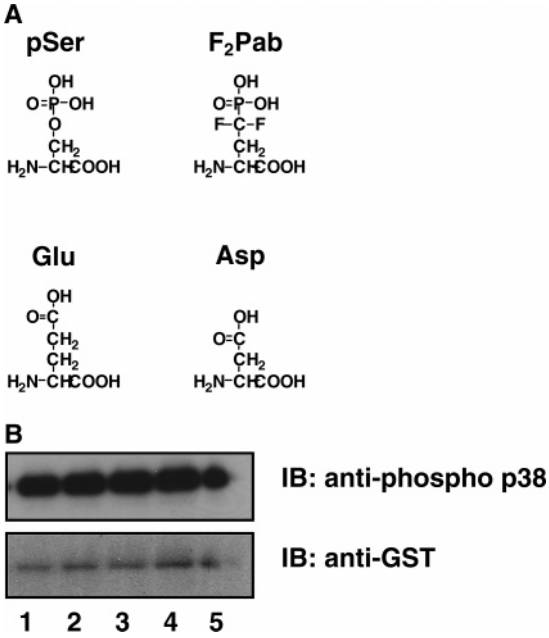

FIGURE 4: Selectivity of cyclic phosphopeptides with phosphoserine or a phosphoserine mimetic. (A) Chemical structures of phosphoserine (pSer), L-2-amino-4-phosphono-4,4-difluorobutanoic acid (F_2-Pab), glutamic acid (Glu), and aspartic acid (Asp). (B) Immunoblot analysis of MKK6-catalyzed phosphorylation of the *N*-terminal GST-tagged, full-length p38α protein with or without cyclic phosphopeptide inhibitors. The phosphorylation states of GST-p38α were analyzed with an anti-phospho-p38 antibody (top panel) that recognizes phosphorylation at T180 and Y182 of p38. The GST-p38α protein level of each reaction was confirmed with an anti-GST antibody (bottom panel). Row 1, no inhibitor; row 2, c(MpSIpYVA); row 3, c(MF_2PabIpYVA); row 4, c(MEIpYVA); and row 5, c(MDIpYVA). The concentrations of GST-p38α, MKK6, ATP, and cyclic phosphopeptide inhibitors were 150 nM, 30 nM, 100 μM, and 100 μM, respectively. All assays were performed at 30 °C and pH 7.5.

To examine the effects of additional phosphoserine mimetics, glutamic acid- and aspartic acid-substituted derivatives also were tested. As expected, c(M**F_2Pab**IpYVA) was not dephosphorylated by PP2Cα, and it effectively inhibited the phosphatase activity of rWip1 (Table 3). Although the IC_{50} value of 16.5 μM (K_i = 4.2 μM) for the inhibition of rWip1 is 4.5-fold weaker than that of c(M**pS**IpYVA), this derivative showed higher activity than other cyclic phosphopeptides (Tables 2 and 3). In contrast to c(M**F_2Pab**IpYVA), the c(M**E**IpYVA) or c(M**D**IpYVA) derivatives did not show significant inhibitory activity against each of the phosphatases (Table 3), suggesting that glutamic acid and aspartic acid do not compensate for phosphoserine.

Because phosphorylation of the pTGpY motif in p38 MAP kinase is catalyzed by MKK6 kinase, an upstream MAP kinase-kinase of p38, there was a possibility that a cyclic phosphopeptide might bind to the catalytic site of MKK6 and inhibit its kinase activity. To explore this possibility, a kinase assay of MKK6 for the *N*-terminal GST-tagged, full-length p38α protein (GST-p38α) with or without cyclic phosphopeptide was performed. Immunoblot analysis of MKK6-catalyzed phosphorylation of GST-p38α showed that none of the four cyclic phosphopeptides with phosphoserine or the phosphoserine mimetic inhibited MKK6 activity (Figure 4B).

Structural Analysis. Docking simulations were conducted to better understand the molecular basis for the observed selectivity of c(MpSIpYVA) for Wip1. For this purpose, we used a homology model of Wip1 (*16*) that was developed from the crystal structure of PP2Cα. Because of the relatively large exposed area of the catalytic site, multiple distinct binding motifs were identified. Figure 5 displays one of the few motifs that were repeated most often among the hundreds of performed simulations. In particular, to emphasize the near perfect reproducibility, Figure 5 displays the superposition of the seven lowest-energy structures of c(MpSIpYVA) obtained from independent groups of simulations. This binding motif is especially interesting because it is analogous to that we previously reported for the linear DEMpTGpYVA substrate peptide (*16*). Specifically, we found that the phosphate group of the phosphoserine residue was in contact with R76 (in approximately the same position as that of the phosphate ion in the PP2Cα crystal structure (*26*)) and that the phosphate group of the phosphotyrosine residue forms salt-bridges with the positively charged side chains of the K238 and/or K218 residues of Wip1. As shown previously (*16*), K238 is unique to Wip1 among the PP2C family, whereas K218 is conserved among the other PP2C members. Intriguingly, in the binding motif shown in Figure 5, the hydrophobic isoleucine between the phosphoserine and phosphotyrosine, which was found to be important for inhibitory activity, projects from the surface, where it could be exposed to solvent and destabilize the complex. In contrast, the hydrophobic valine residue of the cyclic peptide is energetically favorably buried in a nonpolar pocket at the interface of the complex. All attempts to manually position and use docking simulations to find a related binding motif that would additionally locate the isoleucine residue in a nonpolar environment were unsuccessful.

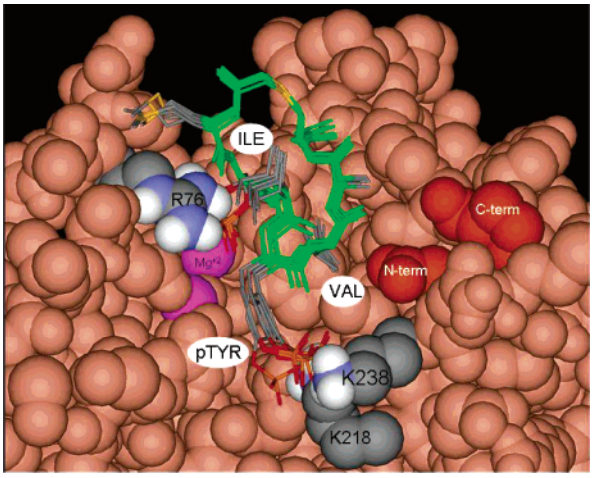

FIGURE 5: Molecular model from docking simulations of Wip1 complexed with c(MpSIpYVA). Seven independently obtained lowest energy structures of a highly populated binding motif of c(MpSIpYVA) are shown superimposed. The color scheme of these cyclic phospopeptides is the same as that in Figure 3B. The homology model of Wip1 is shown in light orange, except for the two Mg^{2+} atoms (magenta) and highlighted residues. Residue labels for the cyclic phosphopeptide are distinguished by white oval backgrounds. The *N*- and *C*-terminal anchors for the missing loop in the homology model that is unique to Wip1 among the PP2C family are shown in dark orange.

Lysine 238 of rWip1 Is Important for the Interaction with the Thioether Cyclic Phosphopeptide. Because molecular modeling indicated that K238 in rWip1 may play an important role in the interaction with c(MpSIpYVA), inhibi-

Table 4: Inhibition of rWip1 Mutants Phosphatase Activities by c(MpSIpYVA)

mutant	IC_{50} (μM)[a]	K_m (μM)[b]	K_i (μM)[c]
WT	3.7 ± 0.2	17 ± 3	0.9
K238Q	623 ± 222	30 ± 4	235
K238D	ND[d]	35 ± 4	ND[d]
R110E	5.7 ± 0.7	13 ± 2	1.5

[a] IC_{50} values for the inhibition of rWip1 mutants by c(MpSIpYVA) were estimated from dose−response phosphatase assays. The results show the average of at least duplicate experiments. Assay conditions were the same as those in Figure 2B. [b] The K_m values for the TDDEMpTGpYVAT substrate peptide were estimated by eq 3. [c] The K_i values were estimated by eq 2 as described in Experimental Procedures. [d] The IC_{50} and K_i values could not be determined because of high IC_{50}.

tion assays with strategic point mutations in rWip1 were undertaken. As was done previously, K238 was changed to glutamine and aspartic acid, which are conserved in the PP2Cα, β, or γ member sequences (*16*). We also tested the R110 mutant (R110E) that has substrate specificity similar to that of wild-type rWip1 (*16*).

The K238Q change resulted in a dramatically elevated IC_{50} value compared to that of wild-type rWip1 (Table 4). The estimated K_i value for K238Q was 235 μM, which is 260-fold higher than that of wild-type rWip1. The K238D mutant was also not inhibited by c(MpSIpYVA). In contrast, the R110E variant showed a K_i value of 1.5 μM, similar to that of wild-type rWip1 (Table 4). We next compared the inhibitory activities of K238Q rWip1 and PP2Cα by the F_2-Pab-containing cyclic phosphopeptide, c(MF_2PabIpYVA). Because of high IC_{50} values, we could not estimate the K_i values against K238Q Wip1 and PP2Cα (results not shown); however, activities could be measured by increasing the inhibitor concentration to 100 μM; these were 27 and 26% for K238Q rWip1 and PP2Cα, respectively. These results suggest that K238 is not only important for its interaction with the cyclic phosphopeptide inhibitor but also for its selectivity with respect to that of other phosphatases.

DISCUSSION

Inhibition of Wip1 activity may suppress the proliferation of certain types of cancer cells (*14*). Furthermore, analyses of *PPM1D* null mice revealed defects in reproductive organs, immune function, and cell cycle control (*34*), indicating that Wip1 must have several important biological functions. Recent studies indicate that in addition to p38 MAP kinase (*2*), UNG2 (*7*), p53 (*8*), Chk1 (*8*), and Chk2 (*9*) are physiological substrates of Wip1; however, the role of Wip1 in regulating the activities of these newly described substrates is not clear. The development of a specific inhibitor of Wip1 is important not only for its use as an anti-cancer drug but also to further clarify the biological role of Wip1 in cell signaling. Recent studies identified inhibitors of Wip1 (*35*) or PP2Cα (*36*) by screening a small chemical compound library or by computational analysis; however, the inhibition mechanism of these compounds has not been elucidated.

Cyclic Phosphopeptide Inhibitor of Wip1. In this study, we designed a phosphopeptide inhibitor for the catalytic site of Wip1 on the basis of its substrate specificity. We found that phosphopeptides containing the pSIpY motif confer higher inhibitory activities among tested peptides. Although many phosphoproteins are known, phosphoproteins with a pSIpY sequence have not been identified. This suggests that a Wip1 endogenous inhibitor with the pSIpY sequence may not exist.

The cyclic phosphopeptide c(MpSIpYVA) was a potent inhibitor (K_i < 1 μM) of rWip1 in a competitive manner. CD and NMR measurements revealed that c(MpSIpYVA) forms a more rigid structure than the linear peptide or the less active cyclic peptides in buffer solution (Figure 3). The high degree of conformational flexibility of the linear peptide may be a cause of lower activity; hence, such peptides were cyclized to decrease conformational flexibility (*17*, *37*). Additionally, cyclic peptides may be resistant to proteases and be more stable than their linear counterparts. Because of these advantages, cyclic peptides are frequently used to design inhibitors of protein−protein interactions (*17*) or of tyrosine phosphatases (*37*).

The structure obtained by NMR measurements showed that the truncation and cyclization of peptides fix the side chains of both phosphorylated residues to be roughly aligned along one side (Figure 3B). The resulting enhanced inhibitory activity indicates that this conformation is especially suitable for binding to the catalytic site of Wip1. We also found that a peptide containing the phosphoserine mimetic F_2Pab showed high inhibitory activity for rWip1 (K_i < 5 μM) (Table 3). More importantly, c(MF_2PabIpYVA) showed >12-fold selectivity toward rWip1 over PP2Cα, which has a catalytic domain that is 50% similar to that of Wip1 (residue 61−378 in humans). The microcystins and the nodularins are naturally occurring cyclic peptides and are potent inhibitors of the catalytic sites of PP1 and PP2A (*15*). Because PP2C family members have different catalytic domain structures compared to those of PP1 and PP2A (*32*), the microcystins and the nodularins would not inhibit the phosphatase activity of the PP2C family (*15*). In addition, there is no structural similarity between cyclic phosphopeptide inhibitors of Wip1 and the microcystin or the nodularin structures; therefore, our cyclic phosphopeptides represent the first specific and potent Wip1 inhibitors to be described.

Interaction of the Cyclic Phosphopeptide Inhibitor with Wip1. As seen in our previously published sequence alignment (*16*), there is a high degree of conservation of the metal-binding and directly adjacent residues (e.g., R76) forming the catalytic sites of Wip1 and PP2Cα. In contrast, sequence substitutions, including E37/P80, Q186/K238, R186/D264, and D243/N318 (in PP2Cα/Wip1) are found farther from the catalytic site. Because the residues in the catalytic site of Wip1 are highly conserved among PP2C family members, it was expected that designing inhibitors specific for the catalytic site of Wip1 would be challenging (*38*). However, our cyclic phosphopeptides clearly demonstrate that the catalytic site of Wip1 is a good target for the development of specific inhibitors. Docking simulations strongly suggest that c(MpSIpYVA) binds to the Wip1 catalytic site in a manner analogous to that of the previously studied DEMpT-GpYVA substrate peptide (see Figure 5 and ref 16 (*16*)). Inhibition studies using rWip1 with specific point mutations provide support for this conclusion. That the inhibitory activity of the cyclic phosphopeptide was progressively reduced for the K238Q and K238D mutants indicates a close contact with phosphotyrosine in c(MpSIpYVA). This also

is consistent with the lack of an effect of the R110E mutant, which is on the opposite side of the active site of Wip1 from K238. Having the same binding motif as that of the substrate is also consistent with the finding presented here, that is, that the mechanism of inhibition for c(MpSIpYVA) is competitive. K238 of Wip1, which is important for the high selectivity of c(MpSIpYVA) (Table 3), is conserved in human, mouse, *Xenopus*, and zebrafish Wip1 but not in other PP2C family members. Therefore, a substrate-based inhibitor that interacts not only with the catalytic site (e.g., R76) but also with the unique residue(s) surrounding it (e.g., K238) is essential for the development of a specific inhibitor of Wip1.

The results of the docking simulations, however, leave the question of the exposed cyclic phosphopeptide isoleucine residue, which would destabilize the complex if in contact with aqueous solvent, unanswered. Interestingly, studies of the TDDEMpS*X*pYVAT series of peptides (Table 1) indicated that not all hydrophobic residues bestow activity equally and that hydrophilic residues do not enhance activity over better hydrophobic residues. These findings suggest the existence of a steric interaction between the residue at this intervening position in the cyclic phosphopeptide sequence and the Wip1 protein. One possible explanation is that the nonmodeled loop of Wip1 (see Experimental Procedures) folds over the catalytic site and buries the isoleucine residue of the cyclic phosphopeptide in a nonpolar enviroment. As seen in Figure 5, the *N*- and *C*-terminal anchors in the model of Wip1 are near enough to the catalytic site for the 25 residues of the loop to reach over and cover the cyclic phosphopeptide in the complex. That this loop is unique to Wip1 among the PP2C family is consistent with the cyclic phosphopeptide being selective for this isoform.

Substrate Specificity of Wip1. Recent studies reported that Wip1 dephosphorylates the phosphoserine in the pSQ sequences of p53 Ser15 and Chk1 Ser345 (*8*) and the phosphothreonine in the pTQ sequence of Chk2 Thr68 (*9*). We also found that the TDDEMpSQpYVAT peptide is a substrate for rWip1 (Table 1). However, in p53 (VEPPL-pSQ-ETFS), Chk1 (QGISF-pSQ-PTCP), Chk2 (LETVS-pTQ-ELYS), and the TDDEM-pSQ-pYVAT peptide, no other amino acids surrounding the p(S/T)Q sequences are conserved. These data indicated that glutamine in the p(S/T)Q sequence is essential for Wip1 substrate recognition. The p(S/T)Q sequence is different from the pT*X*pY sequence previously reported for substrates such as p38 MAP kinase and UNG2, suggesting that Wip1 must distinguish between the pT*X*pY substrates and pSQ substrates. Although p38 MAP kinase and UNG2 were initially found to be physiological substrates (*2*, *7*), other Wip1 substrate proteins with pT*X*pY sequences have not been reported. Moreover, ERK2 and JNK1, which have the pTEpY sequence and pTPpY sequence, respectively, are not substrates for Wip1 (*2*, *16*). In contrast, the p(S/T)Q sequence is a substrate motif for ATM and related kinases (ATR and DNA-PK) that regulate cell cycle checkpoints and DNA repair in response to DNA damage (*39*), and many physiological targets of ATM/ATR have been identified, including p53, Chk1, and Chk2 (*39*, *40*). Although the precise role Wip1 plays in regulating the above substrates has not been determined, identification of the detailed substrate specificity of Wip1 and its inhibitors should provide insight into the mechanisms that regulate multiple pathways of cell growth.

In conclusion, our results show that substrate-based cyclic phosphopeptides are potent competitive inhibitors of Wip1. We also identified a specific residue (K238) within the extended catalytic site of Wip1 that plays an important role in determining inhibitor selectivity over that of the other PP2C family members. Although our cyclic phosphopeptides have four negative charges, which may prevent penetration of the cell membrane, our study should facilitate the development of small compounds that will be useful not only as novel anti-cancer drugs but also for revealing the roles of Wip1 in regulating cellular functions.

REFERENCES

1. Fiscella, M., Zhang, H., Fan, S., Sakaguchi, K., Shen, S., Mercer, W. E., Vande Woude, G. F., O'Connor, P. M., and Appella, E. (1997) Wip1, a novel human protein phosphatase that is induced in response to ionizing radiation in a p53-dependent manner, *Proc. Natl. Acad. Sci. U.S.A. 94*, 6048−6053.
2. Takekawa, M., Adachi, M., Nakahata, A., Nakayama, I., Itoh, F., Tsukuda, H., Taya, Y., and Imai, K. (2000) p53-inducible Wip1 phosphatase mediates a negative feedback regulation of p38 MAPK-p53 signaling in response to UV radiation, *EMBO J. 19*, 6517−6526.
3. Lewis, T. S., Shapiro, P. S., and Ahn, N. G. (1998) Signal transduction through MAP kinase cascades, *Adv. Cancer Res. 74*, 49−139.
4. Sanchez-Prieto, R., Rojas, J. M., Taya, Y., and Gutkind, J. S. (2000) A role for the p38 mitogen-acitvated protein kinase pathway in the transcriptional activation of p53 on genotoxic stress by chemotherapeutic agents, *Cancer Res. 60*, 2464−2472.
5. Bulavin, D. V., Saito, S., Hollander, M. C., Sakaguchi, K., Anderson, C. W., Appella, E., and Fornace, A. J., Jr. (1999) Phosphorylation of human p53 by p38 kinase coordinates N-terminal phosphorylation and apoptosis in response to UV radiation, *EMBO J. 18*, 6845−6854.
6. Kishi, H., Nakagawa, K., Matsumoto, M., Suga, M., Ando, M., Taya, Y., and Yamaizumi, M. (2001) Osmotic shock induces G_1 arrest through p53 phosphorylation at Ser^{33} by activated $p38^{MAPK}$ without phosphorylation at Ser^{15} and Ser^{20}, *J. Biol. Chem. 276*, 39115−39122.
7. Lu, X., Bocangel, D., Nannenga, B., Yamaguchi, H., Appella, E., and Donehower, L. A. (2004) The p53-induced oncogenic phosphatase PPM1D interacts with uracil DNA glycosylase and suppresses base excision repair, *Mol. Cell 15*, 621−634.
8. Lu, X., Nannenga, B., and Donehower, L. A. (2005) PPM1D dephosphorylates Chk1 and p53 and abrogates cell cycle checkpoints, *Genes Dev. 19*, 1162−1174.
9. Fujimoto, H., Onishi, N., Kato, N., Takekawa, M., Xu, X. Z., Kosugi, A., Kondo, T., Imamura, M., Oishi, I., Yoda, A., and, Minami, Y. (2006) Regulation of the antioncogenic Chk2 kinase by the oncogenic Wip1 phosphatase, *Cell Death Differ. 13*, 1170−1180.
10. Li, J., Yang, Y., Peng, Y., Austin, R. J., van Eyndhoven, W. G., Nguyen, K. C. Q., Gabriele, T., McCurrach, M. E., Marks, J. R., Hoey, T., Lowe, S. W., and Powers, S. (2002) Oncogenic properties of *PPM1D* located within a breast cancer amplification epicenter at 17q23, *Nat. Genet. 31*, 133−144.
11. Bulavin, D. V., Demidov, O. N., Saito, S., Kauraniemi, P., Phillips, C., Amundson, S. A., Ambrosino, C., Sauter, G., Nebreda, A. R., Anderson, C. W., Kallioniemi, A., Fornace, A. J., Jr., and Appella, E. (2002) Amplification of *PPM1D* in human tumors abrogates p53 tumor-suppressor activity, *Nat. Genet. 31*, 210−215.
12. Saito-Ohara, F., Imoto, I., Inoue, J., Hosoi, H., Nakagawara, A., Sugimoto, T., and Inazawa, J. (2003) PPM1D is a potential target for 17q gain in neuroblastoma, *Cancer Res. 63*, 1876−1883.
13. Hirasawa, A., Saito-Ohara, F., Inoue, J., Aoki, D., Susumu, N., Yokoyama, T., Nozawa, S., Inazawa, J., and Imoto, I. (2003) Association of 17q21-q24 gain in ovarian clear cell adenocarcinomas with poor prognosis and identification of *PPM1D* and *APPBP2* as likely amplification targets, *Clin. Cancer Res. 9*, 1995−2004.
14. Bulavin, D. V., Phillips, C., Nannenga, B., Timofeev, O., Donehower, L. A., Anderson, C. W., Appella, E., and Fornace, A. J., Jr. (2004) Inactivation of the Wip1 phosphatase inhibits

mammary tumorigenesis through p38 MAPK-mediated activation of the $p16^{Ink4a}$-$p19^{Arf}$ pathway, *Nat. Genet. 36*, 343−350.
15. McCluskey, A., Sim, A. T. R., and Sakoff, J. A. (2002) Serine-threonine protein phosphatase inhibitors: development of potential therapeutic strategies, *J. Med. Chem. 45*, 1151−1175.
16. Yamaguchi, H., Minopoli, G., Demidov, O. N., Chatterjee, D. K., Anderson, C. W., Durell, S. R., and Appella, E. (2005) Substrate specificity of the human protein phosphatase 2Cδ, Wip1, *Biochemistry 44*, 5285−5294.
17. Long, Y.-Q., Lung, F.-D. T., and Roller, P. P. (2003) Global optimization of conformational constraint on non-phosphorylated cyclic peptide antagonists of the Grb2-SH2 domain, *Bioorg. Med. Chem. 11*, 3929−3936.
18. Harder, K. W., Owen, P., Wong, L. K. H., Aebersold, R., Clark-Lewis, I., and Jirik, F. R. (1994) Characterization and kinetic analysis of the intracellular domain of human protein tyrosine phosphatase β (HPTP β) using synthetic phosphopeptides, *Biochem. J. 298*, 395−401.
19. Donella-Deana, A., Boschetti, M., and Pinna, L. A. (2003) Monitoring of PP2A and PP2C by phosphothreonyl peptide substrates, *Methods Enzymol. 366*, 3−17.
20. Cheng, Y.-C., and Prusoff, W. H. (1973) Relationship between the inhibition constant (K_I) and the concentration of inhibitor which causes 50 per cent inhibition (I_{50}) of an enzymatic reaction, *Biochem. Pharmacol. 22*, 3099−3108.
21. Shaka, A. J., Lee, C. J., and Pines, A. (1998) Interactive schemes for bilinear operators − application to spin decoupling, *J. Magn. Reson. 77*, 274−293.
22. Palmer, A. G., III, Cavanagh, J., Wright, P. E., and Rance, M. (1991) Sensitivity improvement in protein-detected 2-dimensional heteronuclear correlation NMR-spectroscopy, *J. Magn. Reson. 93*, 151−170.
23. Hwung, T.-L., and Shaka, A. J. (1995) Water suppression that works − excitation sculpting using arbitrary wave-forms and pulsed-field gradients, *J. Magn. Reson. A112*, 275−279.
24. Delaglio, F., Grzesiek, S., Vuister, G. W., Zhu, G., Pfeifer, J., and Bax, A. (1995) NMRPipe: a multidimensional spectral processing system based on UNIX Pipes, *J. Biomol. NMR 6*, 277−293.
25. Schwieters, C. D., Kuszewski, J. J., Tjandra, N., and Clore, G. M. (2003) The Xplor-NIH NMR molecular structure determination package, *J. Magn. Reson. 160*, 65−73.
26. Das, A. K., Helps, N. R., Cohen, P. T. W., and Barford, D. (1996) Crystal structure of the protein serine/threonine phosphatase 2C at 2.0 Å resolution, *EMBO J. 15*, 6798−6809.
27. Jackson, M. D., Fjeld, C. C., and Denu, J. M. (2003) Probing the function of conserved residues in the serine/threonine phosphatase PP2Cα, *Biochemistry 42*, 8513−8521.
28. Morris, G. M., Goodsell, D. S., Halliday, R. S., Huey, R., Hart, W. E., Belew, R. K., and Olson, A. J. (1998) Automated docking using a Lamarckian genetic algorithm and empirical binding free energy function, *J. Comput. Chem. 19*, 1639−1662.
29. Sanner, M. F. (1999) Python: a programming language for software integration and development, *J. Mol. Graphics Modell. 17*, 57−61.
30. Takekawa, M., Maeda, T., and Saito, H. (1998) Protein phosphatase 2Cα inhibits the human stress-responsive p38 and JNK MAPK pathways, *EMBO J. 17*, 4744−4752.
31. Pribic, R., van Stokkum, I. H. M., Chapman, D., Haris, P. I., and Bloemendal, M. (1993) Protein secondary structure from fourier transform infrared and/or circular dichroism spectra, *Anal. Biochem. 214*, 366−378.
32. Jackson, M. D., and Denu, J. M. (2001) Molecular reactions of protein phosphatases-insights from structure and chemistry, *Chem. Rev. 101*, 2313−2340.
33. Chen, L., Wu, L., Otaka, A., Smyth, M. S., Roller, P. P., Burke, T. R., Jr., den Hertog, J., and Zhang, Z. Y. (1995) Why is phosphonodifluoromethyl phenylalanine a more potent inhibitory moiety than phosphonomethyl phenylalanine toward protein-tyrosine phosphatases? *Biochem. Biophys. Res. Commun. 216*, 976−984.
34. Choi, J., Nannenga, B., Demidov, O. N., Bulavin, D. V., Cooney, A., Brayton, C., Zhang, Y., Mbawuike, I. N., Bradley, A., Appella, E., and Donehower, L. A. (2002) Mice deficient for the wild-type p53-induced phosphatase gene (*Wip1*) exhibit defects in reproductive organs, immune function, and cell cycle control, *Mol. Cell. Biol. 22*, 1094−1105.
35. Belova, G. I., Demidov, O. N., Fornace, A. J., Jr., and Bulavin, D. V. (2005) Chemical inhibition of Wip1 phosphatase contributes to suppression of tumorigenesis, *Cancer Biol. Ther. 4*, 1154−1158.
36. Rogers, J. P., Beuscher, A. E., IV, Flajolet, M., McAvoy, T., Nairn, A. C., Olson, A. J., and Greengard, P. (2006) Discovery of protein phosphatase 2C inhibitors by virtual screening, *J. Med. Chem. 49*, 1658−1667.
37. Akamatsu, M., Roller, P. P., Chen, L., Zhang, Z. Y., Ye, B., and Burke, T. R., Jr. (1997) Potent inhibition of protein-tyrosine phosphatase by phosphotyrosine-mimic containing cyclic peptides, *Bioorg. Med. Chem. 51*, 157−163.
38. Harrison, M., Li, J., Degenhardt, Y., Hoey, T., and Powers, S. (2004) Wip1-deficient mice are resistant to common cancer genes, *Trends Mol. Med. 10*, 359−361.
39. Kastan, M. B., and Lim, D. S. (2000) The many substrates and functions of ATM, *Nature Rev. Mol. Cell Biol. 1*, 179−186.
40. Zhao, H., and Piwnica-Worms, H. (2001) ATR-mediated checkpoint pathways regulate phosphorylation and activation of human Chk1, *Mol. Cell. Biol. 21*, 4129−4139.

BI061356B